International Journal of Wavelets, Multiresolution
and Information Processing
Vol. 4, No. 2 (2006) 345–356

World Scientific
www.worldscientific.com

MODAL-WAVELET TRANSFORM AS A SMART VISUALIZATION TOOL

HISASHI ENDO*, SEIJI HAYANO† and YOSHIFURU SAITO‡

Graduate School of Engineering, Hosei University
3-7-2 Kajino, Koganei, Tokyo 184-8584, Japan
**endo@ysaitoh.k.hosei.ac.jp*
†*hayano@ysaitoh.k.hosei.ac.jp*
‡*ysaitoh@ysaitoh.k.hosei.ac.jp*

ILIANA MARINOVA

Department of Electrical Apparatus
Technical University of Sofia, Sofia 1756, Bulgaria
iliana@tu-sofia.bg

KIYOSHI HORII

Faculty of Literature, Shirayuri College
Midorigaoka, Chofu 182-8525, Tokyo, Japan
khorii@shirayuri.ac.jp

A method of information processings based on the classical field theory is outlined to derive the modal-wavelet transform (MWT) as a wavelet-like orthonormal transform. The theoretical background and application of MWT are described. The bases of MWT are derived from modal analysis of the potential field equations. Namely, a principal idea of MWT is that a numerical data set is regarded as a set of the field potentials or source densities. A modal matrix, constituting characteristic vectors, derived from the discretized field equations enables us to carry out an orthonormal transform inasmuch as the same way as those of conventional discrete wavelets. MWT is based on this data modeling to provide multiresolution analysis in an efficient manner. Three-dimensional MWT demonstrates a classification of a weather satellite infrared animation into background and cloud-moving frame images.

Keywords: Data representation; modal analysis; wavelets.

AMS Subject Classification: 35R05, 45C05, 65T60

1. Introduction

The spread of high performance and reasonably priced computers has stimulated to establish the large-scale Internet community as well as information resources. Data handling technologies based on digital computers are of main importance to realize more efficient networking and computing. Discrete wavelet transform (DWT) may

be a promise to become a deterministic methodology handling the digital signals and images, e.g., compressing data quantity, extracting their characteristics, etc.[1,2] Moreover, their applications to electromagnetic field calculation, solving forward and inverse problems, have been investigated and spurred to a faster calculation algorithm.[3,4] The conventional DWT, however, sometimes suffers from limitation on subject data size, which must be of power of 2. Thereby, the applications depend on employed wavelet basis, and it needs an enormous memory installation for implementation. The principal purpose of this paper is to derive new wavelet basis to carry out more efficient wavelet analysis.

This paper proposes modal-wavelet transform (MWT, in short) as one of the DWTs. The bases of MWT are derived from a modal analysis of the discretized field equations. Regarding a numerical data set as the potential or source density distribution leads to a discretized data model, i.e. the data set can be represented by the field equation like the Poisson equation. Then, the modal analysis of the discretized field equation gives a modal matrix constituting characteristic vectors. The modal matrix enables us orthonormal transforms in the same nature as DWT. MWT employs this matrix as one of the wavelet bases. Because we employ the field equations as data modeling, MWT makes is possible to generate an optimal basis to the subject data size.

2. Modal-Wavelet Transform

2.1. *Data representation by means of field theory*

To derive a new wavelet basis, we consider a discrete data modeling based on the classical field theory. Namely, a numerical data set is assumed to be the potential or source fields. According to the field theory, a scalar field u caused by source density σ could be obtained by solving the differential equation, i.e. Poisson equation:

$$\varepsilon \nabla^2 u = -\sigma, \tag{2.1}$$

where ε is the medium parameter of the field. Also, the scalar field u can be obtained by fundamental solution:

$$u = \frac{1}{\varepsilon} \int g(r)\sigma \, \mathrm{d}r, \tag{2.2}$$

where $g(r)$ is Green's function and r is the distance from the source to reference points.

Discretization of (2.1) and (2.2) by numerical methods derives the following system of equations:

$$L\mathbf{U} = \mathbf{f}, \tag{2.3}$$

and

$$G\mathbf{f} = \mathbf{U}, \tag{2.4}$$

where $\mathbf{f}$ and $\mathbf{U}$ represent the source density σ and scalar field u in the vector forms, respectively. Moreover, L and G denote the coefficient matrices derived from the Laplacian operator in (2.1) and Green's function in (2.2), respectively.

As an example, let each of pixel values in Fig. 1(a) be a scalar potential assuming the medium parameter ε to be a constant value on the entire field, then applying L or G^{-1} to Fig. 1(a) yields the source density distribution as shown in Fig. 1(b). Solving (2.3) or (2.4) with the source density as vector $\mathbf{f}$ reproduces the image as shown in Fig. 2. In particular, Figs. 1(a) and 2(a) are identical in pixel values. Therefore, our discrete data modeling based on the field equations is capable of representing numerical data sets.[5,6]

(a) (b)

Fig. 1. Source density representation of a 2D image. (a) Original image (128 × 128 pixels); (b) An example of source density (128 × 128 pixels).

(a) (b)

Fig. 2. Image recovery from image source density (128 × 128 pixels). (a) Recovered by Poisson equation (2.3); (b) Recovered by fourdamental solution (2.4).

2.2. *Modal-wavelet transform*

As is well known, the matrices L in (2.3) and G in (2.4) derived by available discretizing methods, e.g., finite elements, etc., become the symmetrical as well as positive definite matrices. In case when the vector $\mathbf{U}$ has q elements, it is possible to obtain the characteristic values λ_i, $i = 1, 2, \ldots, q$, of the matrices L and G, and their respective characteristic vectors $\mathbf{v}_i$, $i = 1, 2, \ldots, q$. The matrix composed of the characteristic vectors $\mathbf{v}_i$, $i = 1, 2, \ldots, q$, as its columns is called the modal matrix:

$$M_q = [\mathbf{v}_1, \mathbf{v}_2, \ldots, \mathbf{v}_q]. \tag{2.5}$$

Because of the orthogonality, it holds following relationship:

$$M_q M_q^T = I_q, \tag{2.6}$$

where the superscript T refers to a matrix transpose and I_q is a q by q identity matrix. The modal matrix derived from the coefficient matrix L or G has the same nature as those of the conventional DWT matrices. Figure 3 illustrates the potential distributions given by the characteristic vectors constituting the matrix M_q in case of a two-dimensional data set model. Consider a two-dimensional rectangular region governed by (2.1), then a coefficient matrix L in (2.3) is constructed by the finite element schemes. The orthonormal matrix M_q derives from the characteristic vectors $\mathbf{v}_i$ of the constructed matrix. The characteristic vectors illustrated in Fig. 3

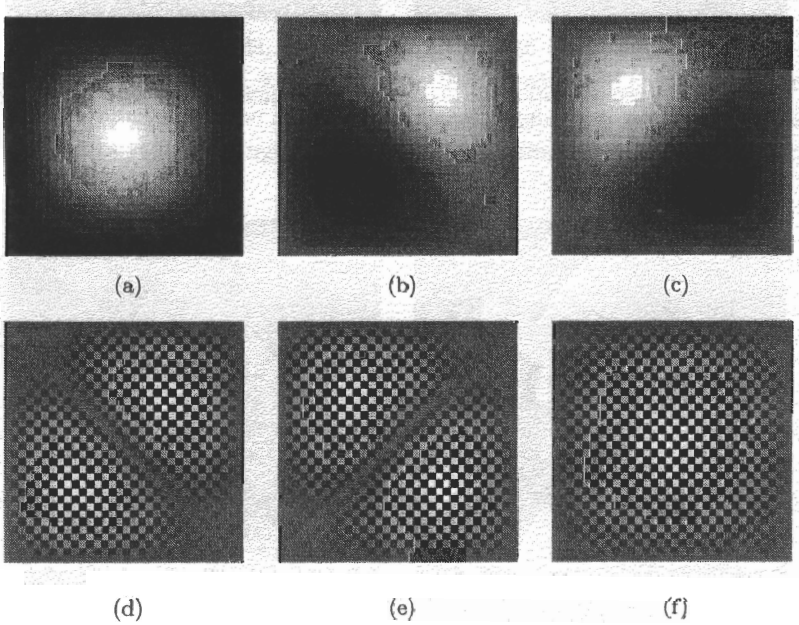

Fig. 3. Images represented by characteristic vectors [30×30 pixels ($q = 900$)]. (a)–(c) $\mathbf{v}_1$–$\mathbf{v}_3$ having the lower level of characteristic values; (d)–(f) $\mathbf{v}_{q-2}$–$\mathbf{v}_q$ having the higher level of characteristic values.

are linearly independent, representing the respective modes in terms of the data set space.[7] A linear combination of the characteristic vectors $\mathbf{v}_i$ is possible to represent the value variation in a data set, just corresponding to the multiresolution orthonormal decomposition of the conventional DWT. Hence, we propose to employ the modal matrix as wavelet-like transform matrices.

2.3. *Transform matrix and basis*

The MWT matrices can be derived by various methods of discretizations. The MWT matrices introduced in the present paper are classified into two types. The first is the differential equation type that assumes a subject data set to be a potential field. The other is the integral expression type that assumes a subject data set to be the field source distribution. At first, let us consider MWT that is derived from the differential equation. The simplest system matrix L can be obtained by a one-dimensional Laplacian operation with equi-spaced three-point finite difference approximation. Namely, the matrix L in (2.3) is given by

$$\nabla^2 u = \frac{\partial^2 u}{\partial x^2} \simeq U_{x-1} - 2U_x + U_{x+1}, \quad x = 1, 2, \ldots, q, \tag{2.7}$$

where the distance of two adjacent data is assumed to be 1. Then, applying the Jacobi method yields a modal matrix M_q in (2.5).[8] Therefore, the dimension of matrix M_q depends on the number of subdivision of (2.7). This means that it is possible to generate an optimal basis having the same data size as that of the subject. In the Laplace partial differential equation, two types of boundary conditions should be considered, i.e. the Dirichlet- and Neumann-type boundary conditions. Figures 4(a) and 4(b) illustrate the typical differential equation-based MWT matrices. As shown in Figs. 5 and 6, the bases constrained the Dirichlet- and Neumann-type boundary conditions to become odd- and even-functions, respectively. The bases of MWT look like sinusoidal functions, however, the bases are not composed of a single frequency component. Moreover, the elements constituting the transform matrices never become the complex numbers like the Fourier transform.

Secondly, let us consider MWT derived from the integral expression. We consider the three-dimensional Green's function $g(r)$ in (2.2). However, the three-dimensional Green's function in cylindrical coordinate system takes infinity when $g(0)$ due to the integral kernel. In order to remove this difficulty, the matrix G in (2.4) is given by assuming the minimum distance $r_{i,i} = 1$, thus,

$$g(r) \simeq \begin{cases} \frac{1}{r_{i,j}} & i \neq j \\ 1 & i = j \end{cases} \qquad i = 1, 2, \ldots, q, \quad j = 1, 2, \ldots, q, \tag{2.8}$$

where the subscripts i and j refer to the source and reference points, respectively. Thereby, $r_{i,j}$ represents the distance between them. Since the system matrix derived from (2.8) becomes symmetrical, then the Jacobi method can be applied to obtain

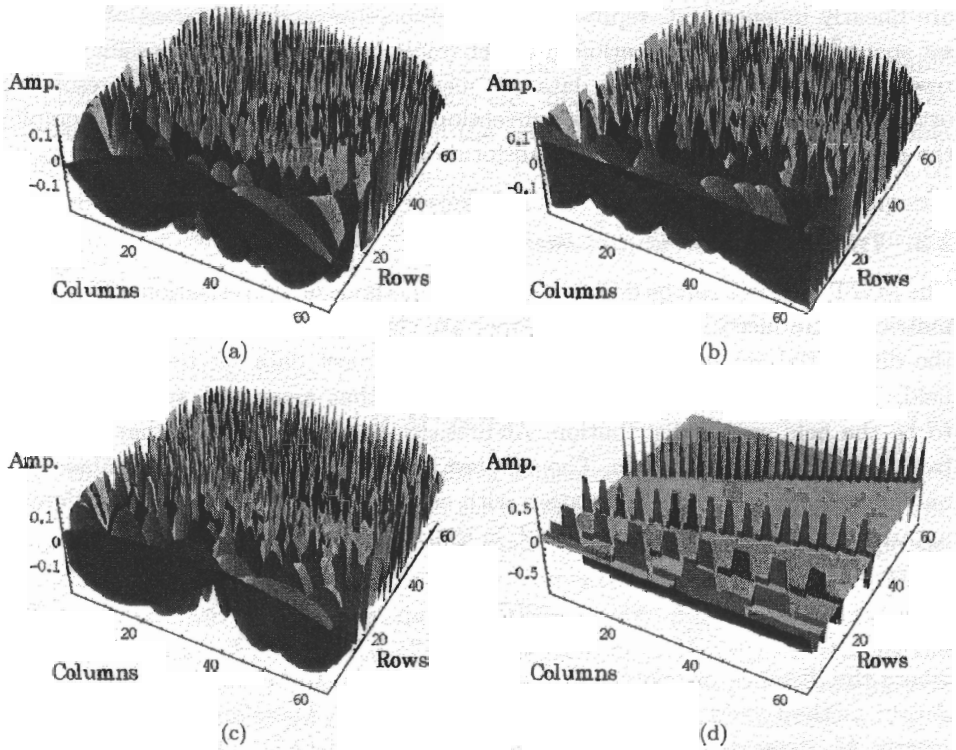

Fig. 4. Modal-wavelet transform matrices (64 × 64). (a) Dirichlet-type boundary condition; (b) Neumann-type boundary condition; (c) Green's function-type; (d) Daubechies 2nd order.

its modal matrix in as much the same way as the MWT based on differential equation. Figures 4(c) and 7 show the MWT matrix and its bases. They have similar patterns to that of the MWT matrix derived under the Dirichlet boundary condition. Figure 8 shows comparison between the MWT and Daubechies 2nd order wavelets along with the spectrum of Fig. 1(a). The transform matrix is non-orthogonal to the subject data set. The major spectrum concentrates around the mother wavelets. It is also the same nature as the cases when the higher-order wavelets are applied.

2.4. *Compressibility*

To compare with the conventional DWT, image compression is carried out. At first, apply MWT or DWT to Fig. 1(a), then the spectrum are obtained. Secondly, neglecting the higher level of obtained spectrum compresses the original data quantity. Finally, image recovery is performed by the inverse of MWT or DWT. To evaluate image recoverability, various compression ratios are applied.

Figure 9 shows comparison of image recovery from 25% compressed image of Fig. 1(a). MWT of Dirichlet-, Neumann- and Green's function-types are compared

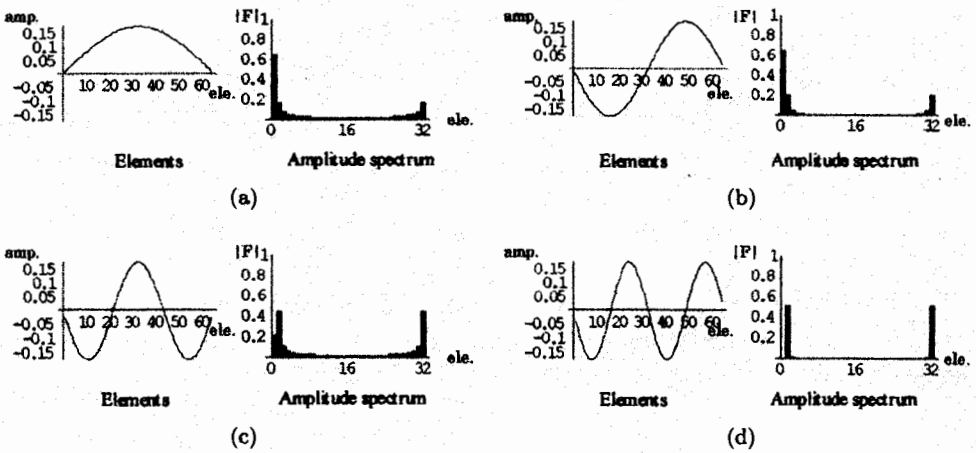

Fig. 5. Elements of the row vectors in the matrix shown in Fig. 4(a) and their Fourier amplitude spectrums. (a)–(d) From the first to fourth row vectors.

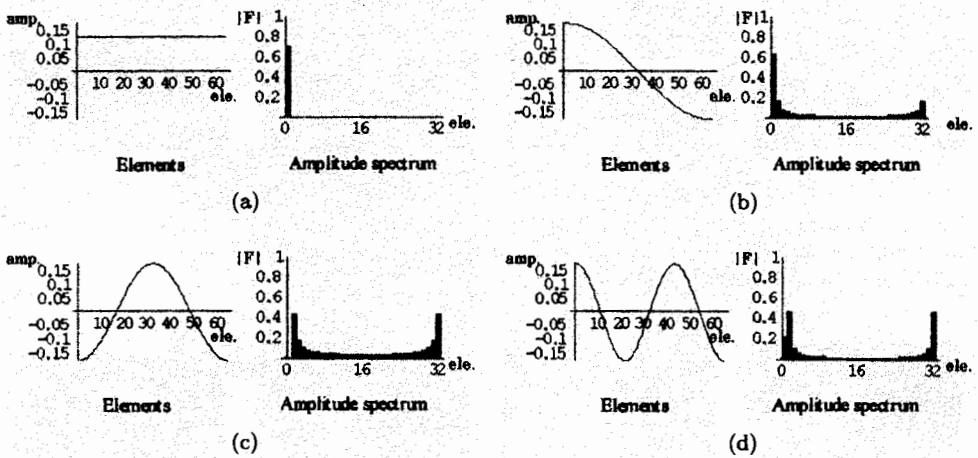

Fig. 6. Elements of the row vectors in the matrix shown in Fig. 4(b) and their Fourier amplitude spectrums. (a)–(d) From the first to fourth row vectors.

with Daubechies 2nd order. According to the frequency characteristics, MWT recovers the smooth images. Correlation coefficients of Figs. 9(a)–(d) are 0.889, 0.935, 0.930 and 0.887, respectively. Fairly good recoverability is revealed in Fig. 10 showing correlation coefficients versus compressed ratios in MWT and DWT. MWT keeps higher recoverability when the data quantity is poor. Moreover, transform matrix of MWT only depends on the subject data length. Thereby, efficient data compression can be performed by MWT derived from the field equations.

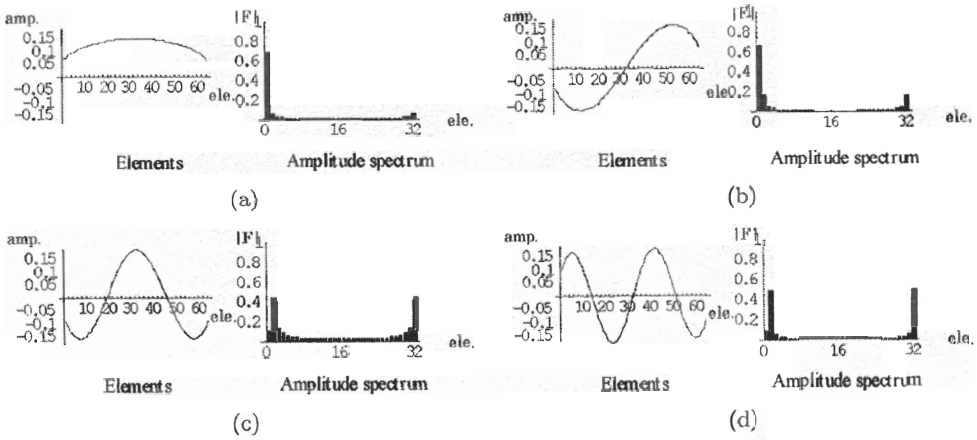

Fig. 7. Elements of the row vectors in the matrix shown in Fig. 4(c) and their Fourier amplitude spectrums. (a)–(d) From the first to fourth row vectors.

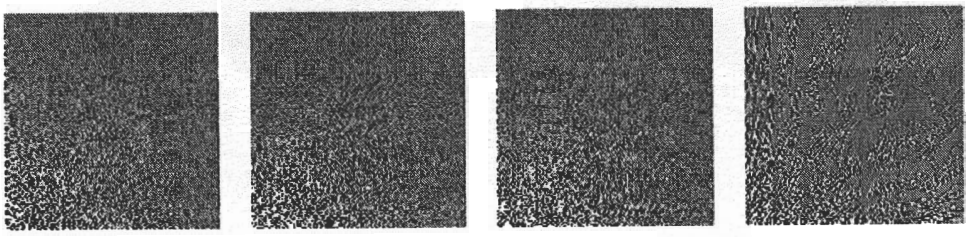

Fig. 8. Wavelet spectrum of Fig. 1(a) (128 × 128 pixels). (a) MWT with Dirichlet boundary condition; (b) MWT with Neumann boundary condition; (c) MWT with Green's function; (d) Daubechies 2nd order.

Fig. 9. Comparison of image recovery from the 25% compressed image of Fig. 1(a) (128 × 128 elements). (a) Dirichlet-type boundary condition; (b) Neumann-type boundary condition; (c) Green's function-type; (d) Daubechies 2nd order.

3. Applications of Animation Image Analysis

3.1. *Infrared animation of weather satellite*

Figure 11 shows some frames of an infrared animation observed by the weather satellite Himawari, showing the generation process of typhoon No. 9 in 2000.[9] Applying

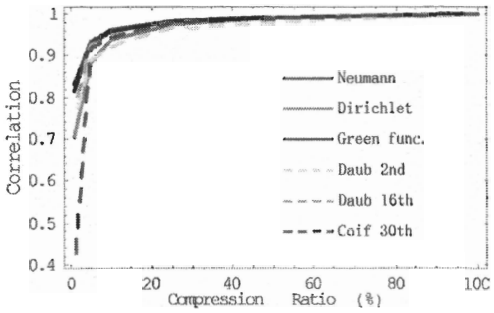

Fig. 10. Correlation coefficients vs. compressed ratios of the image data Fig. 1(a). Neumann-, Dirichlet- and Green's function-types of MWT and Daubechies 2nd, Daubechies 16th, and Coifman 30th-order DWT are evaluated.

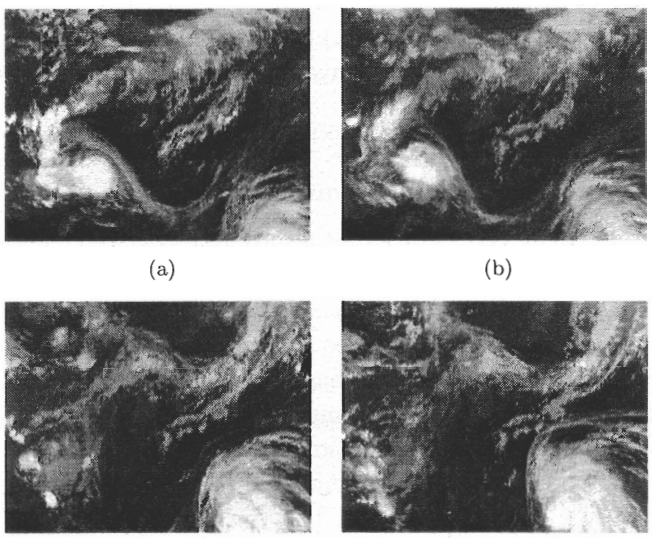

Fig. 11. Frames of infrared animation by weather satellite Himawari (256×193 pixels). (a) At 18:00, August 10th, 2000; (b) At 22:00, August 10th, 2000; (c) At 10:00, August 11th, 2000; (d) At 14:00, August 11th, 2000.

MWT to this animation, separation of static and dynamic images is demonstrated. The animation used in this example is composed of 22 frames captured from 18:00 August 10th to 15:00 August 11th in 2000.

3.2. *Three-dimensional modal-wavelet transform*

In order to carry out MWT to the animation in Fig. 11, the three-dimensional MWT is applied to red, green, and blue color components independently. Namely, applying MWT to horizontal-, vertical- and frame-axes of each color component carries out

animation analysis. Let us consider a one color component of the animation S_{lmn} having $m \times n$ pixels and l frames. Then, its transpose rules are defined by

$$[S_{lmn}]^T = S_{mnl}, \quad [S_{mnl}]^T = S_{nlm}, \quad [S_{nlm}]^T = S_{lmn}. \tag{3.9}$$

The three-dimensional MWT gives the modal-wavelet spectrum S'_{lmn}:

$$S'_{lmn} = \left[M_n \left[M_n [M_l S_{lmn}]^T\right]^T\right]^T, \tag{3.10}$$

where M_l, M_m and M_n are the l by l, m by m and n by n MWT matrices, respectively. And then, inverse MWT recovers the original animation S_{lmn}:

$$S_{lmn} = {M_l}^T \left[{M_m}^T \left[{M_n}^T [S'_{lmn}]^T\right]^T\right]^T. \tag{3.11}$$

Since a linear combination of weighted spectrum represents the original animation S_{lmn}, therefore, animation of each wavelet level can be obtained by means of (3.11).

In this demonstration, (3.10) and (3.11) are independently carried out to each color component. Then, the result of wavelet analysis can be obtained by synthesizing the color images.

3.3. *Separation of static and dynamic images*

As shown in Figs. 4(b) and 6(a), the lowest level of bases derived under the Neumann boundary condition is a constant term. This means that the multiresolution analysis to the frame axis is capable of extracting a common static image through entire frames of animation when employing the Neumann-type MWT matrix. Inasmuch as the same way, the dynamic frame images of animation can be extracted. Figures 12 and 13 show the results of the multiresolution analysis to the frame axis. Taking the lowest level of MWT multiresolution analysis (3.11) into account yields the image in Fig. 12. In this case, the generated result has some frames, but all of frames are identical to Fig. 12. Thus, Fig. 12 is the extracted background image suggesting static air pressure distribution. On the other hand, Fig. 13 shows dynamic frame images of animation obtained by means of (3.11) without the lowest level of

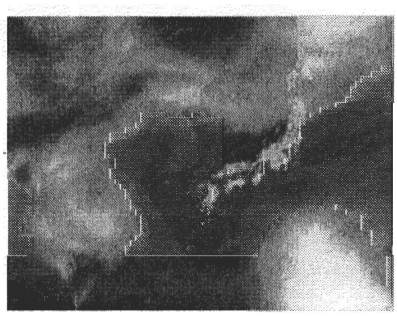

Fig. 12. Extracted static image (256 × 193 pixels).

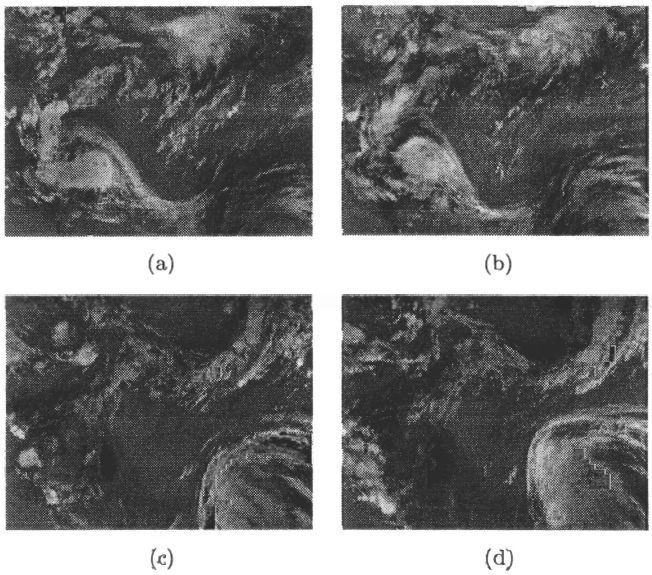

Fig. 13. Frames of extracted dynamic image (256 × 193 pixels). (a) At 18:00, August 10th, 2000; (b) At 22:00, August 10th, 2000; (c) At 10:00, August 11th, 2000; (d) At 14:00, August 11th, 2000.

spectrum. The animation of which pixels vary can be obtained, showing that the cloud is moving.

3.4. *Comparison with the conventional wavelets*

In the conventional DWT, the data sizes l, m and n must be a power of 2. In this animation analysis, the animation shown in Fig. 11 has 256 × 193 pixels and 22 frames. If we carry out the same analysis with conventional DWT, then l, m and n described in Sec. 3.2 become 32, 256 and 256, respectively. In this case, zero-value elements must be added to the original data so that it satisfies these l, m, and n. On the other hand, l, m, and n in MWT are 22, 256 and 193, respectively. MWT dispenses with the arrangement of the original data because the dimension of transform matrix is free from the "*power of 2*" problem. It is obvious that MWT accomplishes an efficient analysis from the viewpoint of memory consumption.

4. Conclusions

We have proposed the MWT and its application of animation analysis. Data representation by field equations has provided the idea to realize the optimal bases to subject data size. The modal analysis to potential field equations has led to the orthonormal matrix having the same nature as those of the conventional wavelets.

An application of animation analysis has demonstrated the separation of static and dynamic images with high efficiency in terms of memory consumption compared with those of the conventional DWT.

Our approach based on the classical field theory is capable of deriving various kinds of orthonormal bases from the governing differential — as well as integral — expressions. Thus, our MWT approach has versatile capability not only to information resource handling but also, to smart computing.

References

1. S. G. Mallat, A theory for multiresolution signal decomposition: The wavelet representation, *IEEE Trans. Pattern Anal. Mach. Intell.* **11** (1989) 674–693.
2. S. Matsuyama *et al.*, Development of n-th dimensional bi-orthogonal wavelets transform and its applications, *J. Vis. Soc. Jpn.* **21** (1999) 347–350 (in Japanese).
3. G. Beylkin *et al.*, Fast wavelet transforms and numerical algorithms, I, *Commun. Pure Appl. Math.* **44** (1991) 141–183.
4. T. Doi *et al.*, An application of the wavelets to the magnetic field source searching, *J. Appl. Phys.* **79** (1996) 4699–4701.
5. H. Endo *et al.*, Image processing by field theory, Part 1: Theoretical background, in *Proc. XIIth Int. Symposium Electr. Apparatus Tech. (SIELA 2001)*, Plovdiv, Bulgaria (2001), pp. 39–45.
6. I. Marinova *et al.*, Image reconstruction for electromagnetic field visualization by an inverse problem solution, *Int. J. Appl. Electromagn. Mater.* **15** (2001/2002) 403–408.
7. P. P. Silvester and R. L. Ferrari, *Finite Elements for Electrical Engineers* (Cambridge University Press, 1983)
8. W. H. Press, B. P. Flannery, S. A. Teukolsky and W. T. Vetterling, *Numerical Recipes in C* (Cambridge University Press, 1988).
9. http://www.jwa.or.jp/